

# Insights into Lightning K-Leader Initiation and Development from Three Dimensional Broadband Interferometric Observations

Daniel Jensen<sup>1</sup>, Xuan-Min Shao<sup>1</sup>, and Richard G. Sonnenfeld<sup>2</sup>

<sup>1</sup>Los Alamos National Laboratory

<sup>2</sup>New Mexico Tech

October 19, 2023

# Insights into Lightning K-Leader Initiation and Development from Three Dimensional Broadband Interferometric Observations

Daniel P. Jensen <sup>1,2</sup>, Xuan-Min Shao <sup>1</sup>, and Richard G. Sonnenfeld <sup>2</sup>

<sup>1</sup>Los Alamos National Laboratory, Los Alamos, NM, USA

<sup>2</sup>Langmuir Laboratory, New Mexico Institute of Mining and Technology, Socorro, NM, USA

## Key Points:

- K-leader propagation often exhibits an initial acceleration followed by a gradual deceleration
- K-leaders often sharply decelerate and then sharply re-accelerate as they approach and pass branch junctions in the flash structure
- A bidirectionally extending region of “twinkling” VHF sources leads to the initiation of the next K-leader

---

Corresponding author: Daniel Jensen, [djensen@alumni.nmt.edu](mailto:djensen@alumni.nmt.edu)

## Abstract

We report detailed observations of K-leaders and the activity between them with the three-dimensional Broadband Interferometric Mapping and Polarization system (BIMAP-3D) at Los Alamos National Laboratory. It is found that K-leaders have a general propagation trend of initial acceleration and then gradual deceleration, and the corresponding very high frequency (VHF) radiation power is exponentially correlated with the leader speed. Based on the 3D development and simultaneous electric field change measurement, some simple K-leaders can be modeled with time-evolving point charges at the propagating leader tip and at the stationary origin. We found that the charge magnitude increases during the initial acceleration stage and stays relatively constant for the rest of the development. K-leaders are observed to interact with other branches; the branches affect the leader's propagation speed, and may affect the charge transfer. After the occurrence of a K-leader, VHF emissions are quenched for several milliseconds. VHF sources then reappear in an impulsive and scattered manner as “twinkling”, and these sources are found not uniquely on the so-called needles, but also on the main channel. These twinkling sources start near the apparent positive leader tip, and extend back towards the direction of the flash origin at about  $10^5$  m/s, while the apparent positive tip continues to extend forward at about  $10^4$  m/s. The twinkling extending towards the direction of flash origin appears to initiate the following K-leader, although it may be interrupted by a K-leader along a different branch, or simply die out without more K-leader activity.

## Plain Language Summary

A K-leader is a discharge process that occurs at the later stage of a lightning flash. It retraces the path established by earlier discharges and propagates at a high speed of  $10^6$ - $10^7$  m/s. Recently we developed a new system called BIMAP-3D that can map lightning radio sources in 3D at a spatial resolution of 10 meters and at a time resolution of a fraction of a microsecond. We found that K-leaders commonly speed up from  $10^6$  to  $10^7$  m/s at the initial stage and then gradually slow down to a stop at their later stage, with associated radio power positively correlated with the traveling speed. Other branches in the lightning flash are found to affect the K-leader speed as it approaches and passes the branch junctions due to charge redistribution caused by the earlier processes. After the occurrence of a K-leader radio emissions are shut off for a few milliseconds due to the increased conductivity of the leader. After that, scattered radio sources reappear in an expanding region, both extending the branch and expanding back towards the starting point of the lightning. These apparent twinkling radio sources lead to the start of the next K-leader.

## 1 Introduction

A K-leader is a lightning discharge process that retraces previously ionized channels in a lightning flash, at speeds on the order of  $10^7$  m/s (Schonland et al., 1935; Loeb, 1966; Jordan et al., 1992; Shao et al., 1995; Shao & Krehbiel, 1996; Stock et al., 2014). K-leaders begin on a channel in the positive breakdown region (typically with net negative cloud charge density) and propagate in the direction of the negative breakdown region (Shao et al., 1995; Stock et al., 2014; Jensen et al., 2021). They are occasionally observed turning “backwards” and propagating back down a different branch in the positive breakdown direction (Stock et al., 2014; Shao et al., 2018, 2023). Recent high speed video observations for occasional out-of-cloud K-leader processes showed that K-leaders start near but not at the tips of the positive breakdown channels (Mazur, 2016; Ding et al., 2022). Very high frequency (VHF) radio observations show a similar initiation location (Hare et al., 2021; Jensen et al., 2021). K-leaders have been observed to commonly slow down as they propagate (Jordan et al., 1992; Stock et al., 2014; Jensen et al., 2021;

Hare et al., 2023), but sometimes to speed up for some fraction of their duration (Stock et al., 2014; Jensen et al., 2021; Hare et al., 2023). The mechanisms behind the changes of speed are not well understood, although Shao and Krehbiel (1996) reported that a K-leader which had a burst of activity near its starting point apparently renewed and intensified the breakdown activity at the negative end.

K-leaders are associated with an electric field change called a K-change (Kitagawa, 1957). Winn et al. (2011) compared New Mexico Tech’s Lightning Mapping Array (LMA) observations with a balloon-borne electric field change measurement, and suggested that the field change is related to a relatively higher charge concentration at the propagating leader tip. In this study the field change will be examined against the 3D K-leader development to better understand the charge distribution along the channel while the leader is propagating forward.

The process of K-leader initiation is even less well understood than the details of K-leader development and dynamics. K-leaders are observed to start in the positive breakdown region, but unlike K-leaders themselves positive leaders are quiet at VHF and difficult to map (Shao et al., 1999; Edens et al., 2012; Pu et al., 2021; Stock et al., 2023). VHF observations by Hare et al. (2019;2021) in this region have been attributed primarily to other processes such as needles around the channel rather than to the actual positive leader tips. High speed video observations have provided insight into K-leader initiation and development when it occurs outside of the cloud. All of these optical observations show evidence of channel cutoff prior to K-leader initiation. That is, at the time when the K-leader becomes visible the connecting channel structure is optically dark, suggesting the channel is relatively cold and low in conductivity (Kong et al., 2008; Saba et al., 2008; Warner et al., 2012; Saraiva et al., 2014; Mazur, 2016; Wang et al., 2019; Huang et al., 2021; Jiang et al., 2022; Ding et al., 2022).

As noted by Jensen et al. (2021), there is a disagreement within the lightning community about the proper terminology for the K-leader phenomenon. In Kitagawa (1957) where the term K-change was coined, the step-like field changes were attributed to processes similar to both recoil streamers and dart leaders. The leader associated with a K-change was later called a K streamer/leader (Shao et al., 1995; Stock et al., 2014). All three terms (dart leader, K-leader, recoil streamer/leader) and minor variations on them continue to be used today in the community (Winn et al., 2011; Stock et al., 2014; Akita et al., 2010; Hare et al., 2021) despite their generally recognized equivalence (Kitagawa, 1957; Shao et al., 1995; Mazur, 2002; Stock et al., 2014; Mazur, 2016). A more complete discussion of the terminology and its history can be found in Rakov and Uman (2003) sections 4.10 and 9.5, Zhu et al. (2014), and Stolzenburg et al. (2015) section 6. In this paper we will exclusively use the term “K-leader” to refer to this phenomenon.

## 2 The BIMAP-3D System

We have recently introduced the Broadband Interferometric Mapping And Polarization in 3D (BIMAP-3D) system at Los Alamos National Laboratory (LANL). BIMAP-3D consists of two stations separated by 11.5 km. Each station consists of four dual-polarization VHF antennas (20-80 MHz), which are combined to provide 2D source location and polarization measurements. Results from the two stations are combined to give 3D location and polarization measurements. In this paper we will focus on the 3D location results. In a favorable scenario when a lightning flash occurs at high altitude between the two stations K-leader channels can be mapped with a resolution of 10 m or better in the three coordinate directions (easting, northing, and altitude) (Shao et al., 2023). Each BIMAP-3D station also has a fast electric field change sensor, or fast antenna.

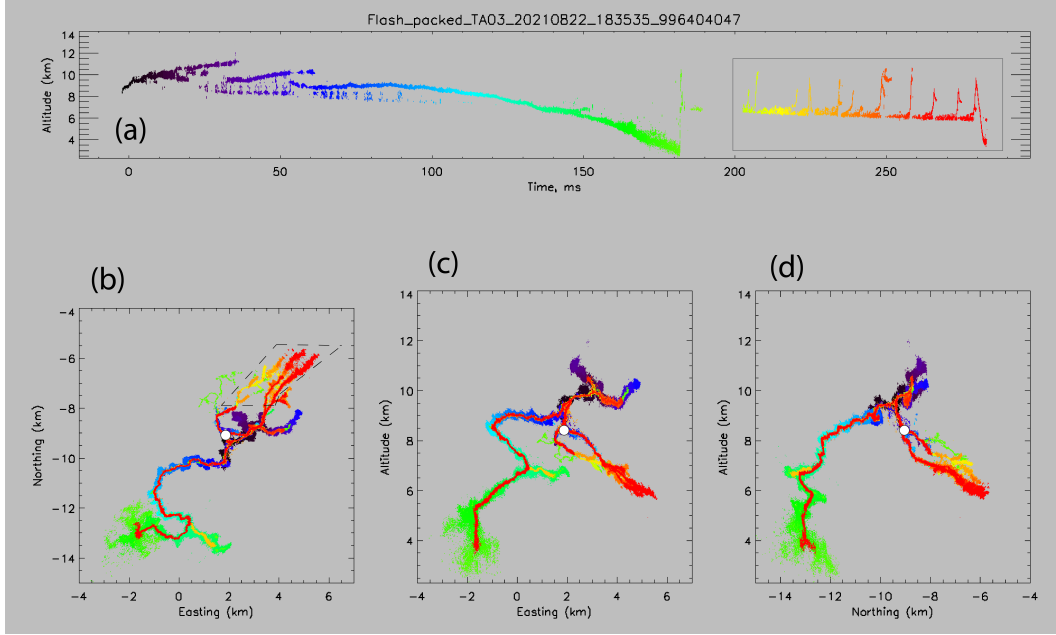


**Figure 1.** Overview of the presented flash, showing altitude (relative to sea level) vs time (a), northing vs easting (b), altitude vs easting (c), and altitude vs northing (d). The origin (zero) of the Easting/Northing coordinate system is defined as the position of the center antenna of the BIMAP1 station, while a white dot marks the flash origin point in panels b, c, and d. The K-leaders in the later part of the flash are boxed in panel a, and a region in panel b is marked with a dashed outline for closer inspection later in Section 6.

### 3 Flash Overview

The K-leaders presented in this paper occurred in a hybrid intra-cloud/cloud-to-ground (IC/CG) bolt-from-the-blue flash, and the flash’s overall structure and development were reported earlier by Shao et al. (2023), as shown in Figure 1. Animation 1 in the supplementary material also provides an overview of the full flash development (Jensen et al., 2023). The flash begins as a typical IC, with the negative stepped leader growing upward. After about 20 ms scattered sources descend to around 8 km altitude (Figure 1a). Beginning at 50 ms, one of the negative leader branches grows from the origin to the southwest and eventually reaches the ground at about 180 ms, at a horizontal distance of 5.5 km from the flash origin. As the return stroke travels back up, it produces VHF sources at the tips of many earlier channels and branches, indicating that it attempts to neutralize previously deposited charge along these channels and branches. In addition, some new, fast-propagating, and positive breakdown branches were produced by the return strokes, e.g., the lime green branches in the region of 1 and 2 km easting and -6.5 and -8 km northing in Figure 1, similar to that reported in Shao et al. (1995).

The data gap between 190 ms and 205 ms is due to a lack of trigger in our instrumentation, suggesting any activity during this period was relatively quiet in VHF. After 200 ms nearly continuous activity extends the positive discharge region to the northeast while descending from 7.5 km to 6.5 km altitude. This gradual descent is periodically interrupted by 14 K-leaders which each rapidly retrace part of the existing channel structure. Most of the observed K-leaders occurred high above the ground in the cloud as normal intra-cloud K-leaders. The last K-leader in the data record propagated near to the ground along the initial leader channel but stopped at 2 km above the ground.

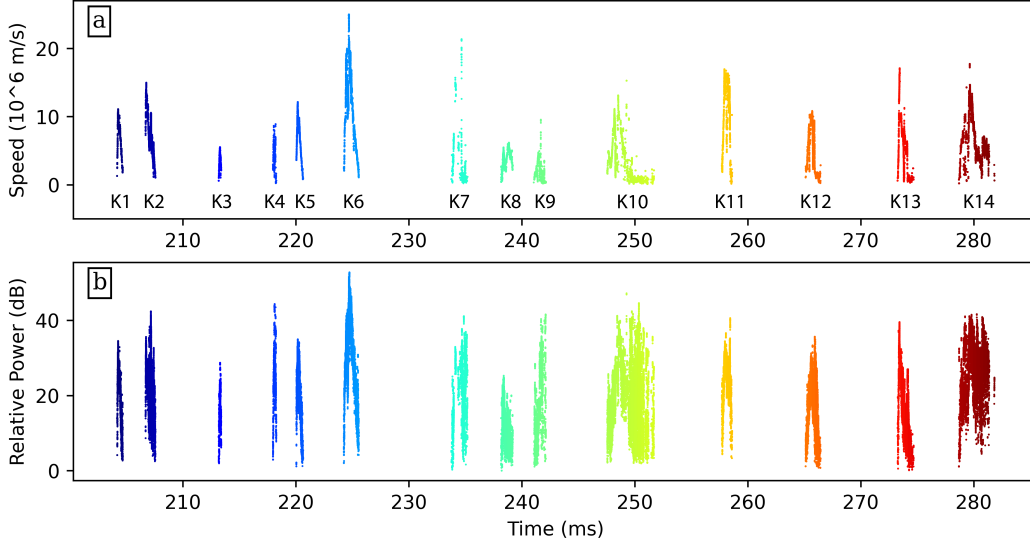


**Figure 2.** Plot of speed vs time (a) and VHF power vs time (b) for all the K-leaders from the analyzed flash. The K-leaders are labeled K1 through K14.

In this paper, we will investigate the K-leader and the inter-K-leader activities, marked with a box in Figure 1a. Animation 2 in the supplementary materials provides a clear view of the 3D development in this later portion of the flash (Jensen et al., 2023).

## 4 K-leader VHF Power and Propagation Speed

### 4.1 Overview of All K-leaders

Since we have not thoroughly calibrated our VHF antennas and the specific BMAP receivers, we will not present VHF power in an absolute scale in this study. Instead, a relative measure of signal to noise ratio (SNR) will be used (Shao et al., 2020). In this case the “noise” level is determined by the lowest received power level among all the analyzed K leaders. SNR for each located source is referenced to this noise level, and is adjusted by the distance from the source to the antennas. Since the results presented only concern trends of increasing and decreasing VHF power the lack of absolute calibration should not affect the validity of our conclusions.

To estimate K-leader propagation speed, a linear fit of the source position vs. time was taken in the three coordinate directions ( $x, y, z$ ) respectively, giving a velocity vector ( $V_x, V_y, V_z$ ). The leader propagation speed is computed from the corresponding velocity vector. The linear fits were calculated in time windows of  $\pm 15 \mu\text{s}$  centered on each source. In order to exclude errors in the velocity calculation caused by sources from multiple simultaneous branches, we restricted sources to be within 500 m of each centered source. Under conservative estimates, the one sigma uncertainty in the speed calculations is  $10^5$  m/s, at least an order of magnitude lower than all of the measured K-leader speeds, and is sufficiently low for this study. Appendix A provides full detail on how the speed uncertainty was calculated.

Figure 2a shows an overview of the speed and power vs time for all the K-leaders, and labels them K1 through K14. The path of each K-leader is shown in Animation 2 in the supplementary materials (Jensen et al., 2023). As illustrated in Figure 2a, the K-leaders typically start and end at a lower speed, reaching a higher speed somewhere in

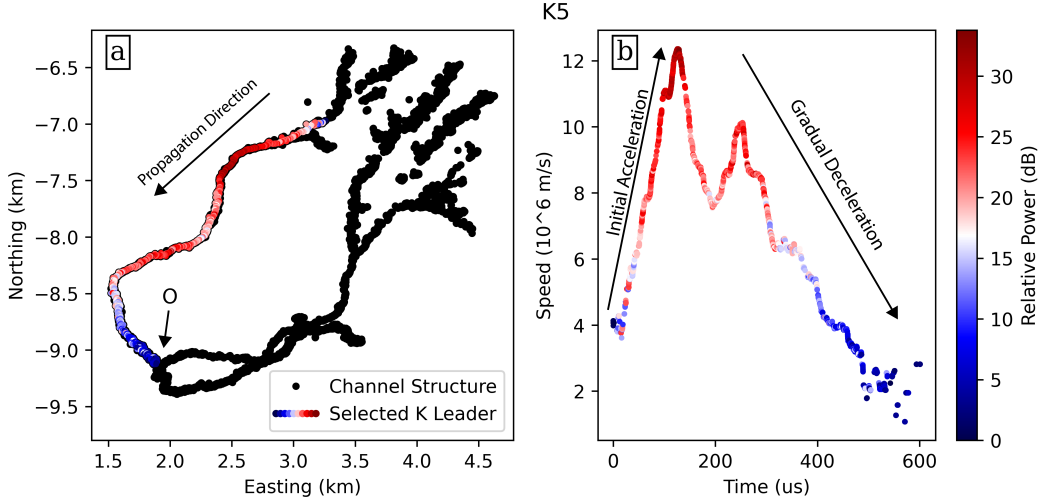


**Figure 3.** Plot of the path of the fifth K-leader (K5) with the background channel structure in Northing vs Easting (a), and the speed of K5 vs time (b). The K-leader sources in both panels are colored by relative VHF power. The flash origin is marked O, along with an arrow for the general propagation direction from the outer branches towards the origin. The first order trends of initial acceleration and gradual deceleration are also marked in panel b. The background channel structure in this figure is a zoomed in view of the full channel structure shown later in Figure 5.

the middle of their propagation, sometimes with significant variations throughout. A similar speed trend was reported by Jensen et al. (2021), although two of the leaders in that study apparently started near their maximum speed. The K-leaders analyzed by Hare et al. (2023) also generally follow these speed trends, although it is clear that individual K-leaders may deviate from the trends for part or all of their development.

Figure 2b shows relative VHF power vs time for these K-leaders. The same general trend as that of the propagation speed is observed. They commonly start and end with lower power levels and reach a higher power level in the middle of their development, apparently correlated with the speed of K-leader propagation. In a few cases the VHF power stayed high while the propagation speed has dropped down toward the end of the propagation, as seen for K10 and K14. These cases apparently correspond to a transition from a normal K-leader propagation to a more step-like propagation mode. This seems to be fairly common at the end of a K-leader's development, K7, K12, and K13 show similar behavior for their last 500  $\mu$ s or so with an average propagation speed of around  $1 \times 10^6$  m/s. We infer the occurrence of stepping at the final stage of the K-leaders because of the observed large variations of VHF power and oscillations in the apparent propagation speed around a relatively constant and slower average speed. These features are similar to that of negative stepped leaders. The speed is also in agreement with the average dart-stepped leader speed of  $(1 - 2) \times 10^6$  m/s reported in Table 1.1 of Rakov and Uman (2003). We could not map any discrete structures associated with the individual steps due to the spatial and temporal resolutions of our current observations. This apparent stepping propagation is marked in the supplementary figures (Jensen et al., 2023).

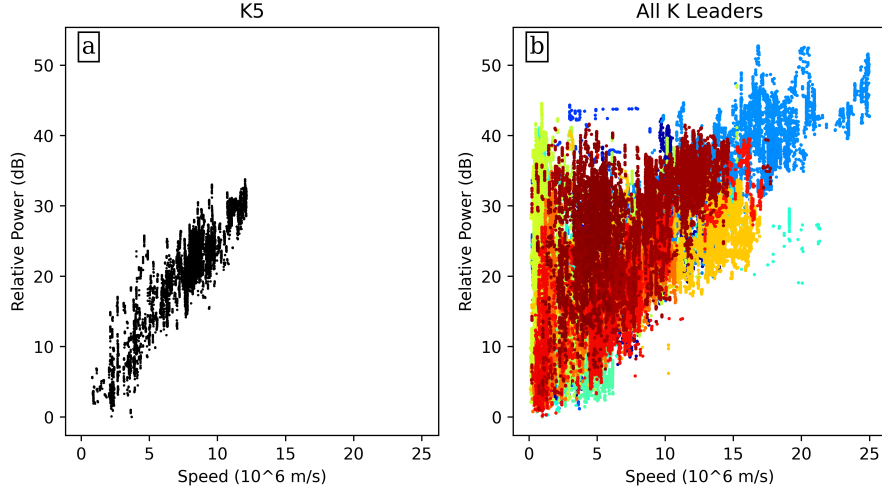


**Figure 4.** Plot of relative power vs speed for K5 (a), and and for all K-leaders, colored by time (b).

## 4.2 Detailed Analysis of a Well Defined K-leader

We now examine the fifth K-leader (K5 in Figure 2) for detailed analysis. K5 propagates along a single branch and has a relatively simple speed behavior. Figure 3a shows the path of K5, extending about 3 km, with points colored by VHF power. In this plot the black dots show the background channel structure for this part of the flash. Figure 3b shows the speed vs. time of K5, again colored by VHF power. This simple K-leader clearly shows a strong initial acceleration from  $4 \times 10^6$  m/s to its maximum speed of  $12 \times 10^6$  m/s in the first  $150 \mu\text{s}$ . It then gradually decelerates to  $2 \times 10^6$  m/s over the remaining  $450 \mu\text{s}$ , until the K-leader sources cease altogether. During the deceleration there is a temporary re-acceleration from  $200 \mu\text{s}$  to  $250 \mu\text{s}$ . Speed variations like this are common and in some cases may overwhelm the typical acceleration or deceleration of the K-leader. Since the general dynamics of K-leaders are still not well understood we will focus on first order trends and leave other variations to future investigations. In general the way the speed of this K-leader changes over time is similar to those reported by Jensen et al. (2021) and Hare et al. (2023).

Figure 3b shows a strong correlation between the leader's speed and power, with the source power starting low, increasing to near its maximum at  $150 \mu\text{s}$ , and then dropping back down to the lowest power level toward the end of the K-leader. The relative power level for this K-leader changed from 0 to about 30 dB across its development.

Figure 4a shows the relative VHF power vs propagation speed for K5. The apparent linear relation between the propagation speed and the logarithmic power indicates an exponential relationship between the two parameters. These results are similar to those recently reported by Hare et al. (2023). Figure 4b is similar to Figure 4a but for all K-leaders in the flash (Figure 2). At low speed there seems to be a wide range of VHF source powers. However, much of this apparent scatter is due to the transition from smoother K-leader propagation to a more step-like propagation as noted for K10, K14, and several others. The correlation between VHF power and speed is still readily apparent at higher speeds for all 14 K-leaders. Apparently in the step-like propagation mode K-leaders can emit significantly higher VHF power than a more smoothly propagating K-leader at the same speed.



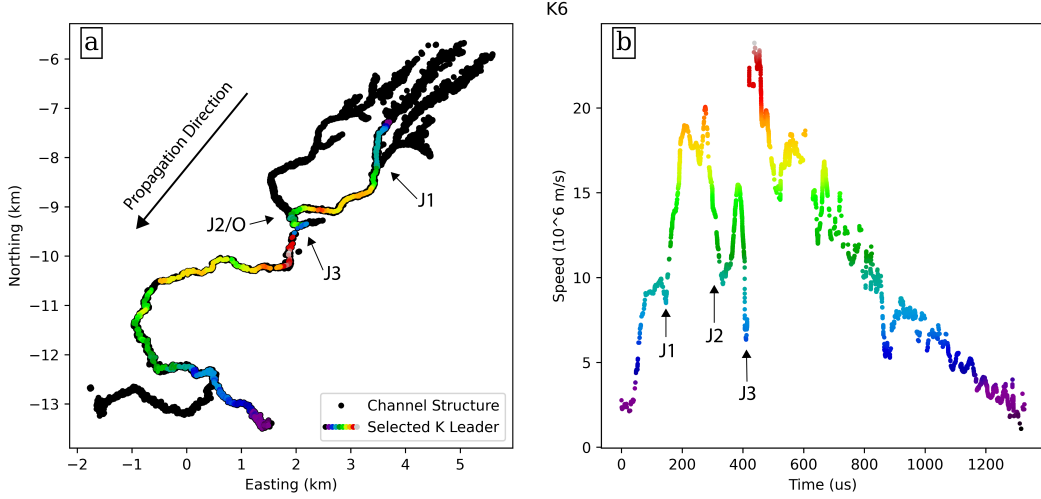


**Figure 5.** A plot of the path of the 6th K-leader (K6) relative to the overall branching structure in Easting vs Northing (a), and the speed of K6 vs time (b), with the K-leader points colored by speed. The junctions J1, J2, and J3, are marked in both panels. J2 is also at the flash origin, marked O. The general propagation direction is indicated with an arrow, K6 begins in the north and ends in the south end of the plot. This figure shows the full background channel structure for the flash, Figure 3 showed only the portion north of -9.5 km northing.

### 4.3 Effect of Branch Junctions on K-leader Speed

In the previous example we examined a K-leader propagating along a single branch. Figure 5 on the other hand shows the 6th K-leader (K6, Figure 2), which passes two branch junctions, or intersections. We now examine whether branch junctions affect the K-leader propagation speed. The black dots in Figure 5a now show the full background channel structure for the flash, whereas in Figure 3 only the northern portion of the channel structure was shown. The upper branch (extending from J3, Figure 5a) has been truncated to avoid the false appearance of junctions. This truncated branch is at higher altitude than the other branches but overlays them in easting and northing (Figures 1c and 1d). The K-leader path in Figure 5a and the points in Figure 5b are colored by speed.

K6 starts with a rapid initial acceleration from  $1.5 \times 10^6$  m/s up to  $9 \times 10^6$  m/s, and then reaches a speed plateau around 100  $\mu$ s. This occurs as the K-leader approaches the first junction (J1). After passing J1 the K-leader rapidly accelerates again up to  $20 \times 10^6$  m/s. The K-leader then decelerates to  $10 \times 10^6$  m/s as it approaches the second junction at the flash origin (J2/O) around 320  $\mu$ s. After passing J2 the K-leader accelerates to  $15 \times 10^6$  m/s at 385  $\mu$ s, before decelerating to  $6 \times 10^6$  m/s as it approaches the third junction (J3) at 410  $\mu$ s. The K-leader then rapidly reaches its maximum speed of  $25 \times 10^6$  m/s at 430  $\mu$ s, before gradually decelerating to  $2 \times 10^6$  m/s at 1300  $\mu$ s. Variations occur within the gradual deceleration, but investigations into the nature of these variations will be left to future research.

The pattern observed is that when the K-leader approaches a branch junction it decelerates, and after it passes a junction it accelerates. Similar behavior has been observed for many other K-leaders in this flash, figures for these K-leaders are included in the supplementary material (Jensen et al., 2023). These common propagation behaviors are an interesting observation and can be explained as the following (Figure 6). We assume the K-leader speed is approximately proportional to the electric field strength at

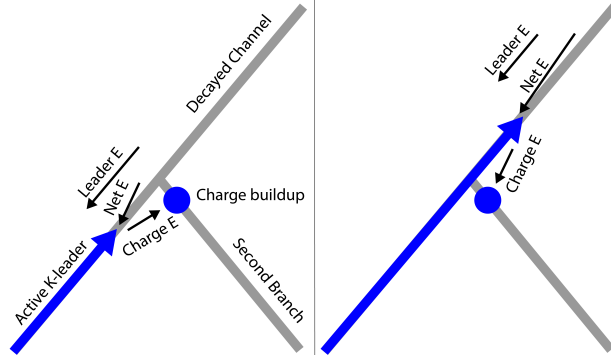


**Figure 6.** A simple diagram showing the hypothesized interaction of a K-leader with a charge deposit near a branch junction. “Leader E” is the electric field vector due to the negative K-leader, “Charge E” is the electric field vector due to the negative charge buildup near the junction, and “Net E” is the net electric field vector at the K-leader tip as the sum of the leader and charge field vectors. The length of each vector indicates the magnitude. As the K-leader approaches the junction the fields from the leader tip and deposited charge destructively interfere ( $|Net \vec{E}| < |Leader \vec{E}|$ ). As the K-leader passes the junction the fields change to constructively interfere ( $|Net \vec{E}| > |Leader \vec{E}|$ ). We assume K-leader speed is approximately proportional to the tip electric field magnitude. This diagram shows the simple case where there is no conductive connection between the branches.

the leader tip. When the branches are inactive prior to the K-leader, the channels are apparently poorly conductive. For different branches that have been active (conductive) alternately at different times, significant potential differences could be built between the branches, and this potential difference will lead to a charge deposit near the branch junction. If the deposited charge is negative, when the active K-leader approaches the junction the electric field at the leader tip will be decreased by the deposited charge, and this will slow down the active K-leader. Once the K-leader passes the junction the deposited charge along the inactive channel will on the other hand increase the field at the leader tip, leading to re-acceleration of the K-leader. It is also possible that the active K-leader increases the conductivity of the inactive branch while passing the junction. In this case, the conductive connection at the junction may further enhance the field at the passing K-leader tip and help to speed up the propagation even more. If the charge deposit at the branch junction is instead positive we would expect the opposite effect (acceleration followed by deceleration). If there is no significant charge deposit the junction is expected to have no effect on the speed. Between Figure 5 and the supplementary figures (Jensen et al., 2023) we have labeled 21 branch junction crossing where the leader speed during the crossing is well defined. Of these, only 2 cases appear to show little to no effect, the other 19 match the negative junction charge pattern.

This interpretation of the deceleration when a K-leader approaches a junction is further supported by K1, K3, and K5, which all stop at the first junction they meet. K1 and K3 can be seen in Animation 2 and their corresponding figures in the supplementary material (Jensen et al., 2023). As reported previously in 2D interferometer observations (Shao & Krehbiel, 1996) and more recently in 3D observations (Shao et al., 2023), shorter K-leaders often stopped at a branch junction, indicating that sufficient negative charge was deposited near or at the junction points to reduce the electric field below the breakdown threshold at the leader tip.

In addition to the branch junction effect, other minor speed variations are observed throughout the K-leader development. We cannot point to a single factor that may cause these variations. We leave analysis of these variations to future investigations.

## 5 K-leader Electric Field Change

Two fast antennas are deployed with the BIMAP-3D system, one at each station. The two fast antennas have different effective gains due to the deployment setup. A relative calibration was achieved between the two fast antennas by comparing the magnitude of field changes for distant flashes (around 50 km from each station). Based on this comparison the fast antenna at BIMAP2 is more sensitive than that at BIMAP1 by a factor of 2, with an estimated uncertainty of 10%.

The amplifiers in the fast antennas also had different time constants (0.2 ms and 1 ms), and the recorded field changes were “de-drooped” accordingly (Sonnenfeld et al., 2006; Födisch et al., 2016). The field change for each K-leader was de-drooped separately and the average field for a time period of 100  $\mu$ s before each K-leader was set to zero. The fast antenna signals were lowpassed at 50 kHz to focus on the electrostatic field component.

Using the recorded field changes from both stations, we modeled the electric field as being produced by a point charge at the leader tip. An opposite point charge was placed at the origin of the K-leader for charge conservation. This charge arrangement is a greatly simplified approximation of the charge distribution expected for an equipotential K-leader channel (Kasemir, 1960; Mazur & Ruhnke, 1998). The ground is assumed to behave like an infinite conducting plane. Then for a sensor located at a point  $(X, Y, Z)$ , where  $Z$  is the ground altitude at the station, the vertical electric field due to the two point charges at a given time is given by

$$E = \frac{-Q}{2\pi\epsilon_0} \left( \frac{z_1 - Z}{(x_1 - X)^2 + (y_1 - Y)^2 + (z_1 - Z)^2} - \frac{z_0 - Z}{(x_0 - X)^2 + (y_0 - Y)^2 + (z_0 - Z)^2} \right) \quad (1)$$

where  $(x_1, y_1, z_1)$  stands for the K-leader tip,  $(x_0, y_0, z_0)$  stands for the K-leader origin, and  $Q$  is the charge at the two points.

The magnitude of the charge  $Q$  in Equation 1 at a given time was estimated using a weighted least-squares fit between the two recorded field changes, accounting for the speed-of-light time delay between the leader tip and the respective fast antennas. The weighting was based on the total change of the field for the entire K-leader recorded by each fast antenna to avoid over-fitting to the closer antenna.

Figure 7 shows the modeled field at each station compared to the measured field (panels a and b) for K5, along with the variation in the modeled charge over time (panel c). The velocity and power over time are also included in the bottom panel (d) for comparison. As shown in Figure 7, the point charge model is a good first order fit to the measured field changes at both stations for K5. The modeled charge increases initially and then stays relatively constant for the rest of the K-leader duration. It is also observed that the increase in charge is generally correlated with the initial propagation acceleration and VHF power increase at the beginning of the K-leader.

It is important to note that this level of fit was only achieved for two of the K-leaders from this flash. Figure 7 shows the fit for K5, which propagated along a single branch (Figure 3). Similar results were observed for K1 (Figure 2), which travels along the same branch. K3 also developed along a single branch and showed similar charge behavior, but the quality of the fit to the measured fields changes was worse. This is possibly be-

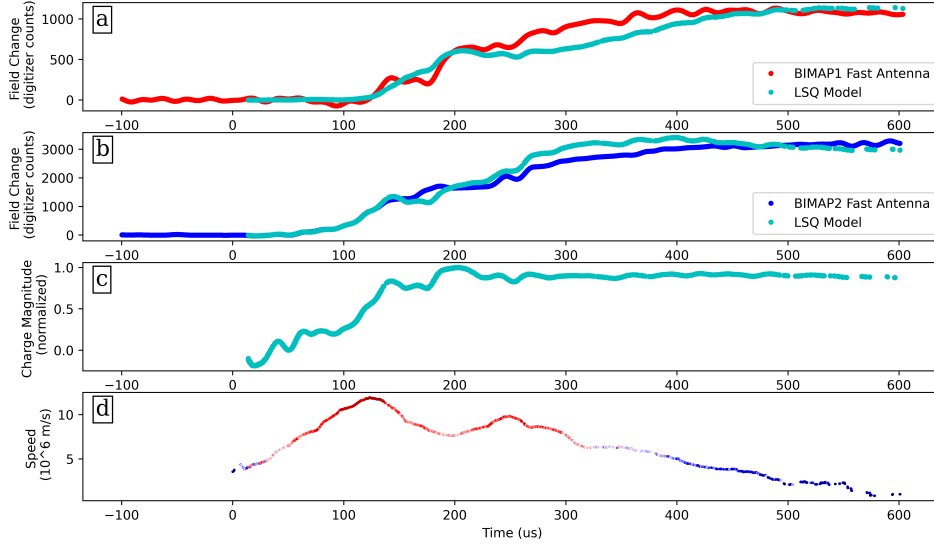


**Figure 7.** Plot of electric field change for K5 at BIMAP1 vs time (a), showing both the measured field change (red) and modeled field change (turquoise). Electric field change at BIMAP2 vs time (b), showing both the measured field change (blue) and modeled field change (turquoise). Modeled charge magnitude vs time (c), and speed vs time (d), colored by power.

cause the field change for K3 was small, and thus more dominated by local noise. The other K-leaders all pass multiple branch junctions (Figure 5, and supplementary figures (Jensen et al., 2023)), and cannot be fit with the simple two point charge model. In these cases the K-leader may redistribute charge along multiple branches as it passes a junction. Even in the single branch case our two point model may be too simplified to accurately capture the evolution of the charge distribution on the channel, but this is one of the first attempts to explore this behavior.

## 6 VHF Sources Between K-leaders

Figure 8 shows the activity that occurs in the positive discharge region after the return stroke. Figure 8a is a Northing vs. Easting plot of the three main branches, which have been grouped into three separate data sets so that they can be analyzed individually. The region containing these branches is marked out with a dashed border in Figure 1b. The region in Figure 8 has been chosen to include essentially all sources in the positive breakdown region, while excluding the K-leaders themselves as much as possible. The full development of this region, along with the K-leaders initiating from it, can be seen in Animation 2 in the supplementary material (Jensen et al., 2023).

Figures 8b, c, and d show the distance from the sources to the flash origin vs time for the west (red), center (green), and east (blue) branches respectively. The time at which a K-leader is launched on a particular branch is marked with a gray vertical line. In most cases K-leader sources are shown as a nearly vertical cluster that coincides with the gray vertical markers. In some cases, the K-leader initiates just outside of the analyzed region and thus the sources do not appear in Figure 8.

Figure 8 shows three interesting insights into K-leader initiation and development. First, in every case the launch of a K-leader (at the times of the gray lines) is followed by an RF quiet period (typically 1-2 ms but sometimes exceeding 10 ms). The VHF suppression occurs specifically on the branch that launched the K-leader. Other branches

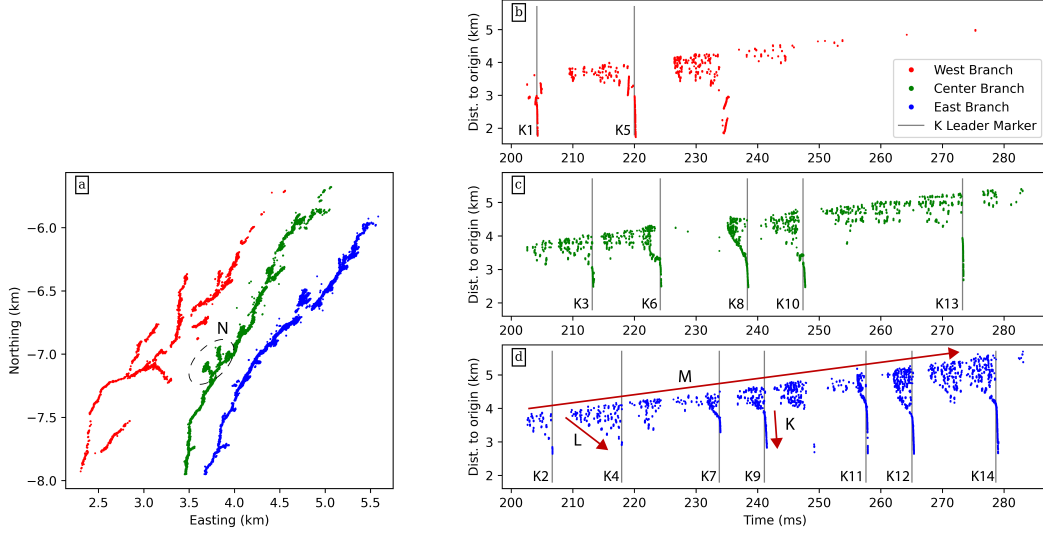


**Figure 8.** Northing vs. Easting plot of three manually separated branches of the positive leader (a), with plots of the distance from the flash origin vs. time for the west (b, red), center (c, green), and east (d, blue) branches. Gray vertical lines on the distance vs. time plots indicate that a K-leader began on that branch at that time. The K-leaders are labeled K1 through K14 chronologically.

may continue to emit VHF, or may also be suppressed. For example, the VHF suppression on the center channel (green, Figure 8c) after K3 does not occur on the other two branches (blue and red). On the other hand, K6 on the center branch (green, panel c) does seem to also suppress the east branch (blue, panel d). Hare et al. (2021) reported similar VHF suppression and referred to it as the K-leader “quenching” the activity on the channel.

Secondly, there appear to be three different types of processes that proceed at three different characteristic speeds. Examples of the three processes are labeled with arrows as K, L, and M in Figure 8d. The best understood, and fastest, of these are the K-leaders themselves, labeled K, typically initiating at speeds on the order of  $10^6$  m/s. The intermediate speed process, labeled L, is suggested by the downward slope at the bottom of each group of sources, and seems to extend at speeds on the order of  $10^5$  m/s. The slowest process is the gentle upward source extension, labeled M, at speeds on the order of  $10^4$  m/s. These three processes will be discussed further in Section 7.3.

Finally, it appears that the possible launch of a K-leader along one branch is sometimes stopped by the initiation of a K-leader on a different branch. For instance the features of the scattered sources after K9 (between 243 ms and 248 ms) along the blue branch (Figure 8d) suggest a K-leader could soon be initiated, but instead K10 along the green branch occurs at this time. K10 apparently suppresses the scattered sources on both branches and appears to stop a K-leader from initiating on the blue branch. Similarly, K6 (green) appears to stop a K-leader on the blue branch. K11 and K12 (blue) also appear to stop K-leaders on the green branch. These observations indicate that neighboring branches can affect each other through the K-leader process.

## 7 Discussion

### 7.1 On Needles and “Twinkling”

We note that there are some small side-branches on the channels in Figure 8a, two examples on the center channel have been circled and labeled N. These small branches are the recently identified needles (Hare et al., 2019; 2021; Pu & Cummer, 2019). Saba et al. (2020) showed high speed video evidence of needles forming as failed branching attempts on upward positive leaders. Saba et al.’s suggested mechanism for needle formation is especially convincing because it explains why needles are typically inclined in the forward direction of the positive leader. In this study essentially all the protrusions from the channels are at  $45^\circ$  or less with the main channel (Figures 8a, 9a, and 9c). This is opposite to the orientation that would be expected if needles were formed originally by the negative end of a cut-off channel as proposed by Hare et al. (2019). The corona-field-reversal mechanism proposed by Pu and Cummer (2019) suggests that needles should be mostly orthogonal to the channel or uniformly distributed around  $90^\circ$ , which is also not consistent with our observations.

Regarding the VHF “flickering”, Stock et al. (2014) reported that positive leaders flickered in a somewhat random way, and Hare et al. (2019) reported that most of these flickering, or “twinkling”, sources are associated with needles. While the claim in Hare et al. (2019) appears to be true for the flash they analyzed, it is not clear that it is true in general. Hare et al. (2019) (their Figure 2) still shows a few twinkling sources that occur along the main channel but not clearly on needles, and the same is true for Hare et al. (2021) (their Figures 20 and 21). Pu and Cummer (2019) also showed many twinkling sources that are arguably on the main positive channel rather than on any needle (their Figure 2).

Our results in this study are shown in Figure 9, for two time intervals (top and bottom) between K-leaders. The left-hand panels (a and c) show the channel structure and location of the twinkling sources in northing vs. easting, where the background channel structure consists of all VHF sources in that region throughout the flash. The right-hand panels (b and d) show the twinkling sources in northing vs. time. In the bottom half of Figure 9a the twinkling sources seem to appear preferentially on the needles. The rest of the twinkling sources in Figures 9a and c seem to appear equally on needles and the main channel. The occurrence frequency of twinkles in Figures 9b and d also appears to be the same between sources on needles and on the channel.

We cannot rule out the presence of needles smaller than our spatial resolution, but in some areas in Figures 9a, and c twinkling sources seem to densely fill the channel. This does not seem consistent with sources occurring on distinct needle branches. Since their appearance in space and time is essentially the same, we consider all of the sources in Figures 8 and 9 to be VHF twinkling, except those associated with K-leaders. Other than appearing more commonly along the main channel our VHF twinkling observations are broadly in agreement with previous reports (Hare et al., 2019; 2021; Pu & Cummer, 2019), although the individual twinkling events are too short in space and time for us to resolve their development.

Regarding the needle structures, our observations of needle orientation relative to the main channel, and high speed video observations of needle formation (Saba et al., 2020), indicate that ionized structures are already present prior to the detection of VHF-visible needles, and the needles sources simply occur on the pre-existing structures. The pre-ionized needle structures are apparently due to failed branching attempts of the VHF quiet positive leader tip. The observations of Hare et al. (2021) that subsequent twinkles on the same needle in general do not extend the needle length is consistent with our interpretation. Based on our observations VHF twinkling is associated with both the nee-

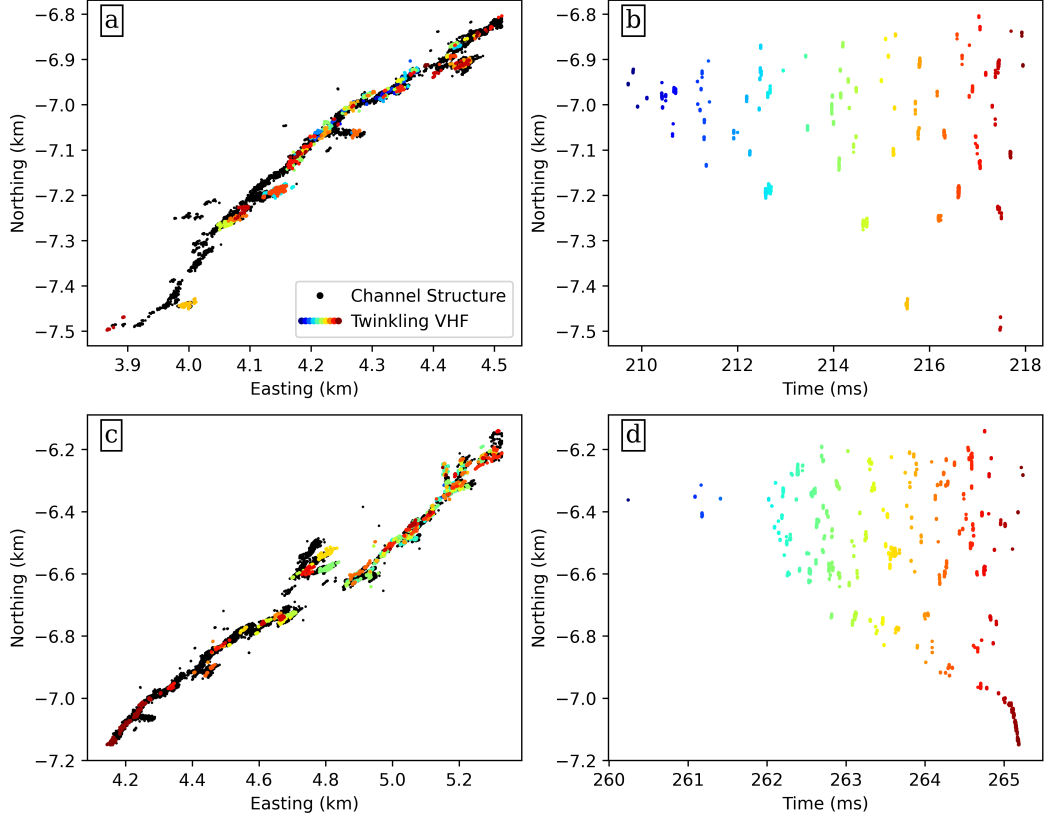


**Figure 9.** Two examples of twinkling behavior between K-leaders. The top panels show the location of twinkling sources and the background channel structure in Northing vs. Easting (a) and twinkling in Northing vs. time (b) for the period between K2 and K4, while the bottom panels show Northing vs. Easting (c), and Northing vs. time (d) for the period between K11 and K12. Both selections are on the east branch of Figure 8. The twinkling sources are colored by time.



dles (failed positive branches) and the main body of the positive channel, which are both part of the pre-ionized channel structure.

As an interesting observation, Figure 9b indicates that the twinkling rate is higher closer to the positive tip (further north in this case), and the distance between twinkling sources also seems to be smaller towards the tip. The fact that the same behaviors are more clear in Figure 9b than Figure 9d may be due to the fact that the majority of the twinkling sources appear within just 2.5 ms in Figure 9d, vs 10 ms in Figure 9b. Pu and Cummer (2019) also reported that the spatial and temporal density of twinkles was highest near the forward tip.

As shown earlier in Figure 8, the downward slope of the southern edge of the twinkling region, and the gentle average upward slope of the northern edge, are both apparent in Figure 9 panels b and d. Our interpretation of these upward and downward slopes will be discussed in Section 7.3.

## 7.2 Quenching vs Masking

With LMA observations of a triggered upward positive leader, Edens et al. (2012) reported that temporal gaps in the positive leader sources seemed to correspond to simultaneous lower altitude negative breakdown. They attributed this to the masking of higher power negative sources over the weaker positive sources. Although this masking could play a role in suppressing VHF sources on the positive leader, K3 in this study (green, Figure 8c) does not interrupt the twinkling on the other two branches (red and blue). There are multiple examples in this flash where a K-leader occurs with simultaneous ongoing VHF twinkling on the other branches. For instance, this occurs for K1 and K5 on the red branch, K8 and K13 on the green branch, and K9 on the blue branch.

We can thus infer that the quenching of VHF sources is a real effect, presumably caused by a change in the physical state of the channel during and after a K-leader. The fact that after quenching the twinkling sources re-start near the apparent positive tip before extending back towards the origin also points to a physical change in the channel conditions.

High speed video observations show K-leaders significantly increasing the channel luminosity (Kong et al., 2008; Saba et al., 2008; Warner et al., 2012; Mazur, 2016; Wang et al., 2019; Huang et al., 2021; Jiang et al., 2022; Ding et al., 2022), indicating increased temperature and conductivity along the channel at that time. Since this is coincident with the suppression of VHF twinkling in this study, we can infer that the increased conductivity is the reason for the VHF quenching. In the cases where a K-leader quenches multiple channels, there must be a conductive connection between those branches. For instance, after K10 on the green branch (Figure 8c) the twinkling along the blue branch (panel d) is also suppressed. Such an inter-connection is consistent with our discussion of K-leaders displacing charge along multiple branches in Section 5, and with our suggestion that a K-leader can interrupt the initiation of other K-leaders (Section 6).

The duration of VHF quenching should therefore be related to the decay time for a conductive K-leader channel to become non-conductive. Shao et al. (2012) predicted that the decay time for a dart leader channel can be approximated as  $\tau = 0.17e^{z/2.3}$  (ms), where  $z$  is altitude in km. At 6 km where the K-leaders started in this study, the decay time would be 2.3 ms. This is surprisingly close to the typical quenching duration observed in Figure 8.

If quenching is caused by the increased conductivity of the K-leader channel, the masking observed by Edens et al. (2012) may have been caused by the same effect. Their observations are generally consistent with the upward positive leader branches producing downward K-leaders, and in some cases these K-leaders may have quenched all the



positive leader branches. On the other hand the LMA is probably more susceptible to masking because of its longer integration windows compared to BIMAP-3D (10  $\mu$ s-100  $\mu$ s compared to  $\sim 0.5$   $\mu$ s).

### 7.3 Three Characteristic Speeds in the Positive Breakdown Region

Among the three characteristic speeds in Figure 8, the fastest is the K-leader itself starting on the order of  $10^6$  m/s (labeled K), which consists of negative breakdown and is clearly visualized by BIMAP-3D. The slowest process on the order of  $10^4$  m/s (labeled M) is associated with the extension of the positive leaders. Since we generally do not see the positive leader tip itself in VHF (Pu et al., 2021; Stock et al., 2023) it is not surprising that this extension seems to continue whether VHF is observed or not. This is most obvious in Figure 8b where very few VHF sources were detected after 250 ms but the upward slope is still apparent. Even though the observed VHF sources are probably not at the positive leader tips, it is reasonable to assume that the true positive leader tip is at a roughly fixed distance ahead. In Figure 8, the average extension speed of all three branches is the same,  $2 \times 10^4$  m/s. It is interesting to note that the occurrence of K-leaders does not appear to have any significant effect on this extension speed.

The intermediate speed process on the order of  $10^5$  m/s (Figure 8d, labeled L) is difficult to interpret. A more detailed view of this development is shown in Figures 9b and d. This speed is associated with the extension of the VHF twinkling region towards the direction of the flash origin, but not related to any well defined channel propagation. Although this extension leads to the start of the next K-leader, with our current observations we do not understand the physical mechanism for this process. Nevertheless this process is clearly associated with K-leader initiation because the downward development in Figures 8c and d generally continues until either a K-leader is initiated or the process is interrupted by a K-leader from another channel.

Optical observations by other researchers show that the channel is dark before a K-leader initiates (Kong et al., 2008; Mazur, 2016; Wang et al., 2019; Huang et al., 2021; Jiang et al., 2022; Ding et al., 2022). In Section 7.2 we argued that VHF twinkling was suppressed on a conductive channel. Taking these together it suggests that the process that causes VHF twinkling and that initiates K-leaders should occur on relatively cold/low conductivity channels.

Hare et al. (2021) and Pu and Cummer (2019) both reported on the forward extension of the twinkling region along a channel with similar distance vs time plots to our Figure 8 (their Figures 22 and 4 respectively). Pu and Cummer (2019) estimated a 2D average speed of  $1 \times 10^5$  m/s for this forward progression, Hare et al. (2021) reports  $5 \times 10^4$  m/s for their case, both are higher than our estimated speed of  $2 \times 10^4$  m/s. In addition, they did not observe the intermediate speed process progressing towards the direction of the flash origin, nor did they report any K-leaders during this interval. In our study the progression towards the flash origin seems to be a feature of twinkling specifically at the stage when K-leaders are being actively produced.

All the VHF twinkling in Figures 8 and 9 is probably the same process we identified as “blooming” in Jensen et al. (2021). The spatial and temporal resolution in Jensen et al. (2021) was insufficient to identify the extension forward and expansion back toward the flash origin, or to make the association with reported observations of VHF twinkling on needles.

### 7.4 Slow Positive Leaders May Generally be Dim

Figures 8 and 9 show scattered VHF twinkling sources in the positive discharge region, and in Section 7.3 we argued that this takes place on a dark channel. Similar VHF twinkling on the positive leader is observed in the early part of the flash, starting 20 ms

into the flash (Figure 1a, around 8 km). The similarity in the source scattering and slow extension ( $\sim 10^4$  m/s) between these two stages of the flash suggests that the positive leader may also be dim in the early part of the flash. Bright positive leaders have been observed in high speed video in other studies, but the reported leader speed is typically one to two orders of magnitude higher ( $10^5$  m/s- $10^6$  m/s) (Saba et al., 2008; Campos et al., 2014; Kong et al., 2015), suggesting the reported optical positive leaders develop under different circumstances as compared to the slow in-cloud development as presented in this paper. Some studies have reported optical observations with evidence of dim or dark positive leaders extending on the order of  $10^4$  m/s (Kong et al., 2008; Wang et al., 2019; Jiang et al., 2022).

## 7.5 The Life Cycle of a K-leader

Based on the observations presented in this paper, the life-cycle in the simplest case is as follows: Following a period of VHF twinkling, a K-leader is initiated. The K-leader then accelerates with increasing charge at both tips, and then the K-leader gradually decelerates to a stop with a relatively constant charge at the tips. After a few milliseconds of VHF quiet period, the twinkling process starts again, and that will lead to the initiation of the next K-leader. We have already discussed the processes leading to the initiation of a K-leader in Section 7.3. We now discuss the physical mechanisms that drive the rest of the K-leader development.

Let us first attempt to explain the initial acceleration of the K-leader. The speed of the K-leader should primarily depend on the electric field strength at the negative leader tip, and the state of conditioning of the channel to be retraced by the K-leader. Since the K-leader channel becomes hot once it is started, as observed optically (Kong et al., 2008; Saba et al., 2008; Warner et al., 2012; Mazur, 2016; Ding et al., 2022), the active leader section can be treated as conductive and approximately equipotential. For an equipotential channel in a uniform electric field the field strength as well as the charge concentration at the tip would increase linearly with channel length (Kasemir, 1960; Mazur & Ruhnke, 1998). In this case it is not difficult to understand the leader acceleration as it propagates forward.

However, at the late lightning stage during the K-leader phase the electric field around the lightning structures cannot be assumed uniform. Earlier discharges prior to the K-leaders have redistributed charge along the channel structures, and the electric field at any position would be a superposition of the general background field and the disturbed field due to the lightning itself. Nevertheless, at the far extremes of the positive breakdown region where the K-leaders are initiated, the local field is likely dominated by the nearby negative charge concentration in the cloud and is less affected by the main lightning structure. In a small spatial scale in this region, the field can be assumed uniform and directed toward the negative charge in the cloud. Under such considerations, the acceleration along a short section of the leader propagation can be understood.

On the other hand, as the K-leader propagates away from the negative cloud charge region and toward the main channel structure the lightning-induced charge redistribution acts as an increasingly more dominant factor. Since previous discharge processes effectively transported negative charge toward the region near and beyond the origin of the flash, the field strength at the active leader tip will be continuously reduced as it propagates toward this region. Under these conditions, the K-leader is expected to slow down after its initial acceleration. This also explains why most K-leaders stop at the origin of the flash and sometimes at branch junctions, especially for simple IC flashes (e.g., Shao and Krehbiel, 1996; Shao et al., 2023). The other factor that helps to slow down the leader propagation is the energy dissipation due to the re-ionization of the pre-established but cold channel, as discussed in Jensen et al. (2021). However, based on the common de-

velopment behavior of the K-leaders it appears that the local field plays a dominant role on its initial acceleration and later deceleration.

## 8 Summary

The results in this paper can be briefly summarized as follows:

1. K-leader propagation speed generally exhibits an initial acceleration followed by a gradual deceleration, though the development of individual K-leaders is often complex.
2. K-leader VHF power is exponentially correlated with speed.
3. K-leaders often enter a step-like propagation mode at around  $1 \times 10^6$  m/s in their final stages, and peak VHF power in this step-like mode can be comparable to the VHF power emitted by K-leaders at their maximum speed.
4. Branch junctions affect K-leader speed, and may affect charge redistribution.
5. In simple cases the K-change can be modeled as time-evolving equal and opposite charges at the K-leader origin and propagating negative tip.
6. The estimated charge magnitude at the K-leader tip increases initially, then stays relatively constant.
7. The initial acceleration and charge buildup of K-leaders can be explained by the equipotential model.
8. The gradual deceleration of K-leaders may be due to charge deposited along the channel by earlier lightning processes.
9. VHF twinkling is not unique to needles, it also occurs on the main channel.
10. We have confirmed that K-leaders quench VHF twinkling, and the quenching is a real physical effect, not an observational artifact.
11. After quenching, the VHF twinkling region extends forward in the positive breakdown direction at  $\sim 10^4$  m/s, and back towards the origin at  $\sim 10^5$  m/s.
12. K-leaders are initiated by the extending twinkling process on an optically dark/low conductivity channel.
13. A K-leader from one branch may interrupt progress towards initiation of a K-leader on other branches.
14. Slow positive leaders ( $\sim 10^4$  m/s) may generally be optically dark while they exhibit VHF twinkling.

## Appendix A Speed Uncertainty Analysis

We can relate the speed uncertainty to the position uncertainty by expressing the speed ( $V$ ) as the difference in time and location of two points

$$V = \sqrt{\left(\frac{x_1 - x_2}{t_1 - t_2}\right)^2 + \left(\frac{y_1 - y_2}{t_1 - t_2}\right)^2 + \left(\frac{z_1 - z_2}{t_1 - t_2}\right)^2} \quad (\text{A1})$$

The uncertainty, expressed as a standard deviation will be of the form

$$\sigma_V = \sum_i \sum_j \left(\frac{\partial V}{\partial i}\right) \left(\frac{\partial V}{\partial j}\right) \sigma_i \sigma_j \quad (\text{A2})$$

where the sums for  $i$  and  $j$  are over each variable,  $x_1, x_2, y_1, y_2, z_1, z_2, t_1$ , and  $t_2$ .

The partial derivatives of  $V$  can be summarized as

$$\frac{\partial V}{\partial x_1} = \frac{1}{V} \frac{x_1 - x_2}{(t_1 - t_2)^2} = \frac{V_x}{V \Delta t} \quad (\text{A3})$$

$$\frac{\partial V}{\partial x_2} = -\frac{1}{V} \frac{x_1 - x_2}{(t_1 - t_2)^2} = -\frac{V_x}{V \Delta t} \quad (\text{A4})$$

$$\frac{\partial V}{\partial t_1} = -\frac{1}{V} \frac{(x_1 - x_2)^2 + (y_1 - y_2)^2 + (z_1 - z_2)^2}{(t_1 - t_2)^3} = -\frac{V}{\Delta t} \quad (\text{A5})$$

$$\frac{\partial V}{\partial t_2} = \frac{1}{V} \frac{(x_1 - x_2)^2 + (y_1 - y_2)^2 + (z_1 - z_2)^2}{(t_1 - t_2)^3} = \frac{V}{\Delta t} \quad (\text{A6})$$

where  $\Delta t = t_1 - t_2$ ,  $V_x = \frac{x_1 - x_2}{\Delta t}$ , and the equations are symmetric for  $x$ ,  $y$ , and  $z$ .

Computing Equation A2 from the partial derivatives, and assuming the uncertainties are the same for both points (i.e.  $\sigma_{x_1} = \sigma_{x_2}$ , etc.), we can see that most of the terms will cancel out since half of the partial derivatives are negative and half are positive. Thus we are left with only the squared terms

$$\sigma_V^2 = \left[ \left( \frac{V_x}{V \Delta t} \right)^2 \sigma_x^2 + \left( \frac{V_y}{V \Delta t} \right)^2 \sigma_y^2 + \left( \frac{V_z}{V \Delta t} \right)^2 \sigma_z^2 + \left( \frac{V}{\Delta t} \right)^2 \sigma_t^2 \right] \quad (\text{A7})$$

If we make a conservative error estimate so that we can assume  $\sigma_x = \sigma_y = \sigma_z = c \sigma_t$ , where  $c$  is the speed of light, then we can combine terms to get

$$\sigma_V^2 = \sigma_x^2 \left[ \frac{1}{\Delta t^2} + \frac{V^2}{c^2 \Delta t^2} \right] \quad (\text{A8})$$

Recognizing that  $\frac{V^2}{c^2} \ll 1$  for any reasonable lightning activity we can drop the second term (associated with  $\sigma_t$ ) and are left with

$$\sigma_V = \frac{\sigma_x}{|\Delta t|} \quad (\text{A9})$$

If we further assume that we have  $N$  points and are taking an average of all of the possible finite differences ( $\frac{1}{2}N(N-1)$  combinations) rather than a single finite difference then we can apply the central limit theorem and get

$$\sigma_{\overline{V}} = \sqrt{\frac{2}{N(N-1)}} \frac{\sigma_x}{|\overline{\Delta t}|} \quad (\text{A10})$$

where  $\sigma_{\overline{V}}$  is the standard deviation of the average speed, and  $\overline{\Delta t}$  is the average time difference between points.

While this averaging method is not identical to the linear fit method used for results presented in Figures 2-5, it is tractable to an analytic solution. The linear fit method was also evaluated via a Monte Carlo simulation.

Parameters for the uncertainty estimation and the resulting uncertainties were determined as follows: Shao et al. (2023) showed that in an ideal case the random location uncertainty of BIMAP-3D can be better than 10 m in all directions ( $x$ ,  $y$ , and  $z$ ). For the purpose of estimating the speed uncertainty we will use a more conservative estimate of 30 m location uncertainty in all directions for the K-leaders analyzed. If we further assume that in a typical 30  $\mu$ s window we have about 30 sources (an underestimate), and the average time difference between sources is about 1/4 the window size, then from Equation A10 we get an estimated speed uncertainty of  $2 \times 10^5$  m/s. A Monte

Carlo simulation was also conducted by repeatedly adding random offsets in each direction (Easting, Northing, and altitude) to each source location and then recalculating the speeds as compared to the non-offset values. For offsets that were normally distributed with a standard deviation of 30 m this method also yielded a one sigma uncertainty of  $2 \times 10^5$  m/s.

Larger speed uncertainties can be caused when sources are coming from multiple branches at the same time, especially when the branches are close to each other so they are hard to separate in the data, but these errors are typically obvious as brief extreme fluctuations in the measured speed and can be excluded from the analysis.

## Appendix B Open Research

All data used for this paper are placed at <https://doi.org/10.5281/zenodo.8213032> (Jensen et al., 2023), along with some supplementary animations and figures. All data files are in text format with headers that describe each data column. A PDF is included which describes the included files, and gives examples of the headers and column format.

## Acknowledgments

Research presented in this article was supported by the Laboratory Directed Research and Development program of Los Alamos National Laboratory under project number 20230223ER.

## References

- Akita, M., Nakamura, Y., Yoshida, S., Morimoto, T., Ushio, T., Kawasaki, Z., & Wang, D. (2010). What occurs in k process of cloud flashes? *Journal of Geophysical Research: Atmospheres*, 115(D7). Retrieved from <https://agupubs.onlinelibrary.wiley.com/doi/abs/10.1029/2009JD012016> doi: 10.1029/2009JD012016
- Campos, L. Z., Saba, M. M., Warner, T. A., Pinto, O., Krider, E. P., & Orville, R. E. (2014). High-speed video observations of natural cloud-to-ground lightning leaders – a statistical analysis. *Atmospheric Research*, 135-136, 285-305. Retrieved from <https://www.sciencedirect.com/science/article/pii/S0169809513000057> doi: <https://doi.org/10.1016/j.atmosres.2012.12.011>
- Ding, Z., Rakov, V. A., Zhu, Y., Kereszy, I., Chen, S., & Tran, M. D. (2022). A positive leader intermittently extending via bidirectional transients and producing a negative cloud-to-ground lightning flash. *AGU Fall Meeting 2022*. Retrieved from [https://agu2022fallmeeting-agu.ipostersessions.com/Default.aspx?s=BC-DB-C9-DA-C0-85-DD-28-4F-E0-9E-65-07-76-EB-D0\(AE35A-0064\)](https://agu2022fallmeeting-agu.ipostersessions.com/Default.aspx?s=BC-DB-C9-DA-C0-85-DD-28-4F-E0-9E-65-07-76-EB-D0(AE35A-0064))
- Edens, H. E., Eack, K. B., Eastvedt, E. M., Trueblood, J. J., Winn, W. P., Krehbiel, P. R., ... Thomas, R. J. (2012). Vhf lightning mapping observations of a triggered lightning flash. *Geophysical Research Letters*, 39(19). Retrieved from <https://agupubs.onlinelibrary.wiley.com/doi/abs/10.1029/2012GL053666> doi: <https://doi.org/10.1029/2012GL053666>
- Födisch, P., Wohsmann, J., Lange, B., Schönherr, J., Enghardt, W., & Kaever, P. (2016). Digital high-pass filter deconvolution by means of an infinite impulse response filter. *Nuclear Instruments and Methods in Physics Research Section A: Accelerators, Spectrometers, Detectors and Associated Equipment*, 830, 484-496. Retrieved from <https://www.sciencedirect.com/science/article/pii/S0168900216305617> doi: <https://doi.org/10.1016/j.nima.2016.06.019>
- Hare, B. M., Scholten, O., Buitink, S., Dwyer, J. R., Liu, N., Sterpka, C., & ter Veen, S. (2023, Jan). Characteristics of recoil leaders as observed by lofar.

- Phys. Rev. D*, 107, 023025. Retrieved from <https://link.aps.org/doi/10.1103/PhysRevD.107.023025> doi: 10.1103/PhysRevD.107.023025
- Hare, B. M., Scholten, O., Dwyer, J., Strepka, C., Buitink, S., Corstanje, A., ... Winchen, T. (2021). Needle propagation and twinkling characteristics. *Journal of Geophysical Research: Atmospheres*, 126(6), e2020JD034252. Retrieved from <https://agupubs.onlinelibrary.wiley.com/doi/abs/10.1029/2020JD034252> (e2020JD034252 2020JD034252) doi: <https://doi.org/10.1029/2020JD034252>
- Hare, B. M., Scholten, O., Dwyer, J., Trinh, T., Buitink, S., Ter Veen, S., ... others (2019). Needle-like structures discovered on positively charged lightning branches. *Nature*, 568(7752), 360–363. doi: <https://doi.org/10.1038/s41586-019-1086-6>
- Huang, H., Wang, D., Wu, T., & Takagi, N. (2021). Recoil leader and associated discharge features observed during the progression of a multi-branched upward lightning flash. *Journal of Geophysical Research: Atmospheres*, 126(24), e2021JD035162. Retrieved from <https://agupubs.onlinelibrary.wiley.com/doi/abs/10.1029/2021JD035162> (e2021JD035162 2021JD035162) doi: <https://doi.org/10.1029/2021JD035162>
- Jensen, D. P., Shao, X.-M., & Sonnenfeld, R. (2023, August). *Data and Supplementary Material for “Insights into Lightning K-Leader Initiation and Development from Three Dimensional Broadband Interferometric Observations” by Jensen et al.* Zenodo. Retrieved from <https://doi.org/10.5281/zenodo.8213032> ([Dataset]) doi: 10.5281/zenodo.8213032
- Jensen, D. P., Sonnenfeld, R. G., Stanley, M. A., Edens, H. E., da Silva, C. L., & Krehbiel, P. R. (2021). Dart-leader and k-leader velocity from initiation site to termination time-resolved with 3d interferometry. *Journal of Geophysical Research: Atmospheres*, e2020JD034309. Retrieved from <https://agupubs.onlinelibrary.wiley.com/doi/abs/10.1029/2020JD034309> doi: <https://doi.org/10.1029/2020JD034309>
- Jiang, R., Yuan, S., Qie, X., Liu, M., & Wang, D. (2022). Activation of abundant recoil leaders and their promotion effect on the negative-end breakdown in an intracloud lightning flash. *Geophysical Research Letters*, 49(1), e2021GL096846. Retrieved from <https://agupubs.onlinelibrary.wiley.com/doi/abs/10.1029/2021GL096846> (e2021GL096846 2021GL096846) doi: <https://doi.org/10.1029/2021GL096846>
- Jordan, D. M., Idone, V. P., Rakov, V. A., Uman, M. A., Beasley, W. H., & Jurénka, H. (1992). Observed dart leader speed in natural and triggered lightning. *Journal of Geophysical Research: Atmospheres*, 97(D9), 9951–9957. Retrieved from <https://agupubs.onlinelibrary.wiley.com/doi/abs/10.1029/92JD00566> doi: 10.1029/92JD00566
- Kasemir, H. W. (1960). A contribution to the electrostatic theory of a lightning discharge. *Journal of Geophysical Research (1896-1977)*, 65(7), 1873–1878. Retrieved from <https://agupubs.onlinelibrary.wiley.com/doi/abs/10.1029/JZ065i007p01873> doi: <https://doi.org/10.1029/JZ065i007p01873>
- Kitagawa, N. (1957). On the mechanism of cloud flash and junction or final process in flash to ground. *Papers in Meteorology and Geophysics*, 7(4), 415–424. doi: 10.2467/mripapers1950.7.4\_415
- Kong, X., Qie, X., & Zhao, Y. (2008). Characteristics of downward leader in a positive cloud-to-ground lightning flash observed by high-speed video camera and electric field changes. *Geophysical Research Letters*, 35(5). Retrieved from <https://agupubs.onlinelibrary.wiley.com/doi/abs/10.1029/2007GL032764> doi: <https://doi.org/10.1029/2007GL032764>
- Kong, X., Zhao, Y., Zhang, T., & Wang, H. (2015). Optical and electrical characteristics of in-cloud discharge activity and downward leaders in positive cloud-to-ground lightning flashes. *Atmospheric Research*, 160, 28–38. Re-



- trieved from <https://www.sciencedirect.com/science/article/pii/S0169809515000721> doi: <https://doi.org/10.1016/j.atmosres.2015.02.014>
- Loeb, L. B. (1966). The mechanisms of stepped and dart leaders in cloud-to-ground lightning strokes. *Journal of Geophysical Research (1896-1977)*, 71(20), 4711-4721. Retrieved from <https://agupubs.onlinelibrary.wiley.com/doi/abs/10.1029/JZ071i020p04711> doi: 10.1029/JZ071i020p04711
- Mazur, V. (2002). Physical processes during development of lightning flashes. *Comptes Rendus Physique*, 3(10), 1393-1409. Retrieved from <https://www.sciencedirect.com/science/article/pii/S1631070502014123> doi: [https://doi.org/10.1016/S1631-0705\(02\)01412-3](https://doi.org/10.1016/S1631-0705(02)01412-3)
- Mazur, V. (2016). The physical concept of recoil leader formation. *Journal of Electrostatics*, 82, 79-87. Retrieved from <https://www.sciencedirect.com/science/article/pii/S0304388616300407> doi: <https://doi.org/10.1016/j.elstat.2016.05.005>
- Mazur, V., & Ruhnke, L. H. (1998). Model of electric charges in thunderstorms and associated lightning. *Journal of Geophysical Research: Atmospheres*, 103(D18), 23299-23308. Retrieved from <https://agupubs.onlinelibrary.wiley.com/doi/abs/10.1029/98JD02120> doi: <https://doi.org/10.1029/98JD02120>
- Pu, Y., & Cummer, S. A. (2019). Needles and lightning leader dynamics imaged with 100-200 mhz broadband vhf interferometry. *Geophysical Research Letters*, 46(22), 13556-13563. Retrieved from <https://agupubs.onlinelibrary.wiley.com/doi/abs/10.1029/2019GL085635> doi: <https://doi.org/10.1029/2019GL085635>
- Pu, Y., Cummer, S. A., & Liu, N. (2021). Vhf radio spectrum of a positive leader and implications for electric fields. *Geophysical Research Letters*, 48(11), e2021GL093145. Retrieved from <https://agupubs.onlinelibrary.wiley.com/doi/abs/10.1029/2021GL093145> (e2021GL093145 2021GL093145) doi: <https://doi.org/10.1029/2021GL093145>
- Rakov, V. A., & Uman, M. A. (2003). *Lightning: physics and effects*. Cambridge university press.
- Saba, M. M. F., Cummins, K. L., Warner, T. A., Krider, E. P., Campos, L. Z. S., Ballarotti, M. G., ... Fleenor, S. A. (2008). Positive leader characteristics from high-speed video observations. *Geophysical Research Letters*, 35(7). Retrieved from <https://agupubs.onlinelibrary.wiley.com/doi/abs/10.1029/2007GL033000> doi: <https://doi.org/10.1029/2007GL033000>
- Saba, M. M. F., de Paiva, A. R., Concollato, L. C., Warner, T. A., & Schumann, C. (2020). Optical observation of needles in upward lightning flashes. *Scientific Reports*, 10(1), 17460. doi: <https://doi.org/10.1038/s41598-020-74597-6>
- Saraiva, A. C. V., Campos, L. Z. S., Williams, E. R., Zepka, G. S., Alves, J., Pinto Jr., O., ... Blakeslee, R. J. (2014). High-speed video and electromagnetic analysis of two natural bipolar cloud-to-ground lightning flashes. *Journal of Geophysical Research: Atmospheres*, 119(10), 6105-6127. Retrieved from <https://agupubs.onlinelibrary.wiley.com/doi/abs/10.1002/2013JD020974> doi: <https://doi.org/10.1002/2013JD020974>
- Schonland, B. F. J., Malan, D. J., Collens, H., & Boys, C. V. (1935). Progressive lightning ii. *Proceedings of the Royal Society of London. Series A - Mathematical and Physical Sciences*, 152(877), 595-625. Retrieved from <https://royalsocietypublishing.org/doi/abs/10.1098/rspa.1935.0210> doi: 10.1098/rspa.1935.0210
- Shao, X.-M., Ho, C., Bowers, G., Blaine, W., & Dingus, B. (2020). Lightning interferometry uncertainty, beam steering interferometry, and evidence of lightning being ignited by a cosmic ray shower. *Journal of Geophysical Research: Atmospheres*, 125(19), e2019JD032273. Retrieved from <https://agupubs.onlinelibrary.wiley.com/doi/abs/10.1029/2019JD032273> (e2019JD032273 2019JD032273) doi: <https://doi.org/10.1029/2019JD032273>

- Shao, X.-M., Ho, C., Caffrey, M., Graham, P., Haynes, B., Bowers, G., ...  
 Rassoul, H. (2018). Broadband rf interferometric mapping and po-  
 larization (bimap) observations of lightning discharges: Revealing new  
 physics insights into breakdown processes. *Journal of Geophysical Re-  
 search: Atmospheres*, 123(18), 10,326-10,340. Retrieved from [https://  
 agupubs.onlinelibrary.wiley.com/doi/abs/10.1029/2018JD029096](https://agupubs.onlinelibrary.wiley.com/doi/abs/10.1029/2018JD029096) doi:  
<https://doi.org/10.1029/2018JD029096>
- Shao, X.-M., Jensen, D., Ho, C., Graham, P., Haynes, W., Caffrey, M., ... Sonnen-  
 feld, R. (2023). Three-dimensional broadband interferometric mapping and  
 polarization (bimap-3d) observations of lightning discharge processes. *Journal  
 of Geophysical Research: Atmospheres*, e2022JD037955.
- Shao, X. M., & Krehbiel, P. R. (1996). The spatial and temporal development of in-  
 tracloud lightning. *Journal of Geophysical Research: Atmospheres*, 101(D21),  
 26641-26668. Retrieved from [https://agupubs.onlinelibrary.wiley.com/  
 doi/abs/10.1029/96JD01803](https://agupubs.onlinelibrary.wiley.com/doi/abs/10.1029/96JD01803) doi: 10.1029/96JD01803
- Shao, X. M., Krehbiel, P. R., Thomas, R. J., & Rison, W. (1995). Radio interfero-  
 metric observations of cloud-to-ground lightning phenomena in florida. *Journal  
 of Geophysical Research: Atmospheres*, 100(D2), 2749-2783. Retrieved from  
<https://agupubs.onlinelibrary.wiley.com/doi/abs/10.1029/94JD01943>  
 doi: 10.1029/94JD01943
- Shao, X.-M., Lay, E., & Jacobson, A. R. (2012). On the behavior of return stroke  
 current and the remotely detected electric field change waveform. *Journal  
 of Geophysical Research: Atmospheres*, 117(D7). Retrieved from [https://  
 agupubs.onlinelibrary.wiley.com/doi/abs/10.1029/2011JD017210](https://agupubs.onlinelibrary.wiley.com/doi/abs/10.1029/2011JD017210) doi:  
<https://doi.org/10.1029/2011JD017210>
- Shao, X. M., Rhodes, C. T., & Holden, D. N. (1999). Rf radiation obser-  
 vations of positive cloud-to-ground flashes. *Journal of Geophysical Re-  
 search: Atmospheres*, 104(D8), 9601-9608. Retrieved from [https://  
 agupubs.onlinelibrary.wiley.com/doi/abs/10.1029/1999JD900036](https://agupubs.onlinelibrary.wiley.com/doi/abs/10.1029/1999JD900036) doi:  
<https://doi.org/10.1029/1999JD900036>
- Sonnenfeld, R. G., Battles, J. D., Lu, G., & Winn, W. P. (2006). Compar-  
 ing e field changes aloft to lightning mapping data. *Journal of Geo-  
 physical Research: Atmospheres*, 111(D20). Retrieved from [https://  
 agupubs.onlinelibrary.wiley.com/doi/abs/10.1029/2006JD007242](https://agupubs.onlinelibrary.wiley.com/doi/abs/10.1029/2006JD007242) doi:  
<https://doi.org/10.1029/2006JD007242>
- Stock, M. G., Akita, M., Krehbiel, P. R., Rison, W., Edens, H. E., Kawasaki, Z.,  
 & Stanley, M. A. (2014). Continuous broadband digital interferometry of  
 lightning using a generalized cross-correlation algorithm. *Journal of Geophys-  
 ical Research: Atmospheres*, 119(6), 3134-3165. Retrieved from [https://  
 agupubs.onlinelibrary.wiley.com/doi/abs/10.1002/2013JD020217](https://agupubs.onlinelibrary.wiley.com/doi/abs/10.1002/2013JD020217) doi:  
<https://doi.org/10.1002/2013JD020217>
- Stock, M. G., Tilles, J., Taylor, G. B., Dowell, J., & Liu, N. (2023). Lightning in-  
 terferometry with the long wavelength array. *Remote Sensing*, 15(14). Re-  
 trieved from <https://www.mdpi.com/2072-4292/15/14/3657> doi: 10.3390/  
 rs15143657
- Stolzenburg, M., Marshall, T. C., Karunarathne, S., Karunarathna, N., & Orville,  
 R. E. (2015). Transient luminosity along negative stepped leaders in light-  
 ning. *Journal of Geophysical Research: Atmospheres*, 120(8), 3408-3435.  
 Retrieved from [https://agupubs.onlinelibrary.wiley.com/doi/abs/  
 10.1002/2014JD022933](https://agupubs.onlinelibrary.wiley.com/doi/abs/10.1002/2014JD022933) doi: <https://doi.org/10.1002/2014JD022933>
- Wang, X., Zhao, X., Cai, H., Liu, G., Liao, M., & Qu, L. (2019). Optical charac-  
 teristics of branched downward positive leader associated with recoil leader  
 activity. *Journal of Atmospheric and Solar-Terrestrial Physics*, 196, 105158.  
 Retrieved from [https://www.sciencedirect.com/science/article/pii/  
 S1364682619304274](https://www.sciencedirect.com/science/article/pii/S1364682619304274) doi: <https://doi.org/10.1016/j.jastp.2019.105158>



- Warner, T. A., Cummins, K. L., & Orville, R. E. (2012). Upward lightning observations from towers in rapid city, south dakota and comparison with national lightning detection network data, 2004–2010. *Journal of Geophysical Research: Atmospheres*, 117(D19). Retrieved from <https://agupubs.onlinelibrary.wiley.com/doi/abs/10.1029/2012JD018346> doi: <https://doi.org/10.1029/2012JD018346>
- Winn, W. P., Aulich, G. D., Hunyady, S. J., Eack, K. B., Edens, H. E., Krehbiel, P. R., ... Sonnenfeld, R. G. (2011). Lightning leader stepping, k changes, and other observations near an intracloud flash. *Journal of Geophysical Research: Atmospheres*, 116(D23). Retrieved from <https://agupubs.onlinelibrary.wiley.com/doi/abs/10.1029/2011JD015998> doi: 10.1029/2011JD015998
- Zhu, B., Zhou, H., Thottappillil, R., & Rakov, V. A. (2014). Simultaneous observations of electric field changes, wideband magnetic field pulses, and vhf emissions associated with k processes in lightning discharges. *Journal of Geophysical Research: Atmospheres*, 119(6), 2699–2710. Retrieved from <https://agupubs.onlinelibrary.wiley.com/doi/abs/10.1002/2013JD021006> doi: <https://doi.org/10.1002/2013JD021006>